# Experimental and computational studies on the reaction of silanes with the diphosphine-bridged triruthenium clusters Ru3(CO)10(μ-dppf), Ru3(CO)10(μ-dppm) and Ru3(CO)9{μ3-PPhCH2PPh(...

**ARTICLE** *in* JOURNAL OF ORGANOMETALLIC CHEMISTRY · SEPTEMBER 2014

Impact Factor: 2.17 · DOI: 10.1016/j.jorganchem.2014.05.040



**9 AUTHORS**, INCLUDING:

Subas Rajbangshi

Jahangirnagar University

**12** PUBLICATIONS **2** CITATIONS

SEE PROFILE

Edward Rosenberg

University of Montana

**172** PUBLICATIONS **2,850** CITATIONS

SEE PROFILE

Michael G Richmond

University of North Texas

**261** PUBLICATIONS **2,289** CITATIONS

SEE PROFILE

Shariff E Kabir

Jahangirnagar University

**224** PUBLICATIONS **2,195** CITATIONS

SEE PROFILE

Journal of Organometallic Chemistry 767 (2014) 185–195

Contents lists available at ScienceDirect

Journal of Organometallic Chemistry

journal homepage: www.elsevier.com/locate/jorganchem

# Experimental and computational studies on the reaction of silanes with the diphosphine-bridged triruthenium clusters $Ru_3(CO)_{10}(\mu$-dppf), $Ru_3(CO)_{10}(\mu$-dppm) and $Ru_3(CO)_9\{\mu_3$-$PPhCH_2PPh(C_6H_4)\}$

Md. Jakir Hossain [a], Subas Rajbangshi [a], Md. Mehedi M. Khan [a], Shishir Ghosh [b], Graeme Hogarth [b, c], Edward Rosenberg [d, **], Kenneth I. Hardcastle [e], Michael G. Richmond [f], Shariff E. Kabir [a, *]

[a] Department of Chemistry, Jahangirnagar University, Savar, Dhaka 1342, Bangladesh
[b] Department of Chemistry, University College London, 20 Gordon Street, London WC1H OAJ, UK
[c] Department of Chemistry, King's College London, Britannia House, 7 Trinity Street, London SE1 1DB, UK
[d] Department of Chemistry, University of Montana, Missoula, MT 59812, USA
[e] Department of Chemistry, Emory University, Atlanta, GA 30322, USA
[f] Department of Chemistry, University of North Texas, Denton, TX 76209, USA

ARTICLE INFO

*Article history:*
Received 26 April 2014
Received in revised form
28 May 2014
Accepted 29 May 2014
Available online 8 June 2014

*Keywords:*
Ruthenium carbonyl
Diphosphine
Silanes
Oxo-capped
Oxidative-addition
X-ray structures

ABSTRACT

Reactions of $Ru_3(CO)_{10}(\mu$-dppf) (**1**) (dppf = 1,1′-bis(diphenylphosphino)ferrocene), $Ru_3(CO)_{10}(\mu$-dppm) (**2**) (dppm = bis(diphenylphosphino)methane), and the orthometalated derivative $Ru_3(CO)_9\{\mu_3$-$PPhCH_2PPh(C_6H_4)\}$ (**3**) with silanes ($Ph_3SiH$, $Et_3SiH$, $Ph_2SiH_2$) are reported. Treatment of **1** with $Ph_3SiH$ and $Ph_2SiH_2$ at room temperature leads to facile Si–H bond activation to afford $Ru_3(CO)_9(\mu$-dppf)$(SiPh_3)(\mu$-H) (**4**) (60% yield) and $Ru_3(CO)_9(\mu$-dppf)$(SiPh_2H)(\mu$-H) (**6**) (53% yield), respectively. The reaction of **1** with $Ph_3SiH$ has been investigated by electronic structure calculations, and these data have facilitated the analysis of the potential energy surface leading to **4**. Compound **1** does not react with $Et_3SiH$ at room temperature but reacts at 68 °C to give $Ru_3(CO)_9(\mu$-dppf)$(SiEt_3)(\mu$-H) (**5**) in 45% yield. Reaction of **2** with $Ph_3SiH$ at room temperature yields two new products: $Ru_3(CO)_9(\mu$-dppm)$(SiPh_3)(\mu$-H) (**7**) in 40% yield and $Ru_3(CO)_6(\mu_3$-O$)(\mu$-dppm$)(SiPh_3)(\mu$-H$)_3$ (**8**) in 15% yield. Interestingly, at room temperature compound **7** slowly reverts back to **2** in solution with decomposition and liberation of $Ph_3SiH$. Complex **8** can also be prepared from the direct reaction between **7** and $H_2O$. Similar reactions of **2** with $Et_3SiH$ and $Ph_2SiH_2$ give only intractable materials. The orthometalated compound **3** does not react with $Ph_3SiH$, $Et_3SiH$ and $Ph_2SiH_2$ at room temperature but does react at 66 °C to give $Ru_3(\mu$-CO$)(CO)_7\{\mu_3$-$PPhCH_2PPh(C_6H_4)\}(SiR_2R^1)(\mu$-H)] (**9**, R = R′ = Ph, 71% yield; **10**, R = R′ = Et, 60% yield; **11**, R = Ph, R′ = H, 66% yield) by activation of the Si–H bond. Compounds **4** and **8**–**11** have been structurally characterized. In **4**, both the dppf and the hydride bridge a common Ru–Ru vector, whereas NMR studies on **7** indicate that two ligands span different Ru–Ru edges. Compound **8** contains a face-capping oxo moiety, a terminally coordinated $SiPh_3$ ligand, and three bridging hydride ligands, whereas **9**–**11** represent simple oxidative addition products. In all of the compounds examined, the triruthenium framework retains its integrity and the silyl groups occupy equatorial sites.



## 1. Introduction

The activation of Si–H bonds by transition metal complexes is a key step in the catalytic process known as hydrosilylation [1–3]. The main entry into M–Si chemistry is by the facile oxidative addition of hydrosilanes to a metal center, and in the case of metal clusters, products with a bridging hydride and terminal silyl groups are produced [4]. Although examples of the ruthenium-carbonyl-catalyzed hydrosilylation using mononuclear complexes exist, fewer reactions of hydrosilanes with ruthenium carbonyl clusters have been published [5]. It has been reported that the reactions of $Ru_3(CO)_{12}$ with hydrosilanes is dependent on the structure of the silane and the reaction conditions, and in many such cases cluster

* Corresponding author. Tel.: +880 27791099; fax: +880 27791052.
** Corresponding author.
*E-mail address:* skabir_ju@yahoo.com (S.E. Kabir).

http://dx.doi.org/10.1016/j.jorganchem.2014.05.040
0022-328X/

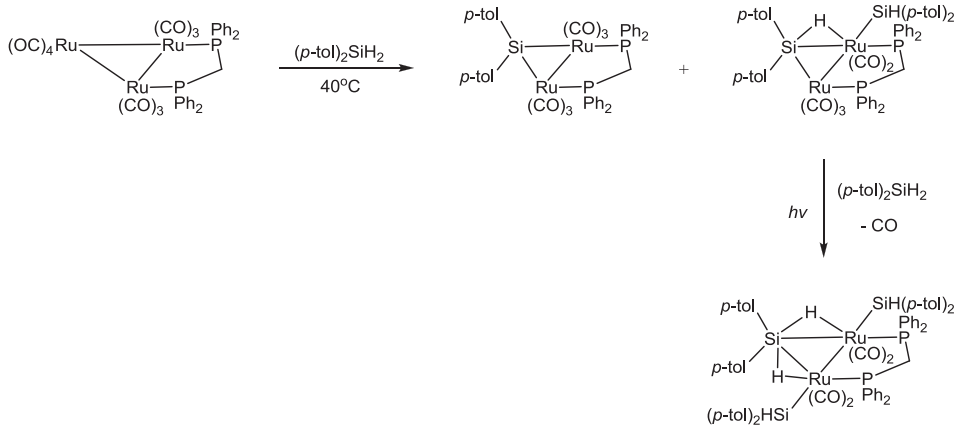


**Scheme 1.**

fragmentation was involved [6]. Lewis et al. reported triruthenium clusters of the type $Ru_3(CO)_{11}(SiR_3)(\mu\text{-}H)$ from the reactions of the labile cluster $Ru_3(CO)_{11}(NCMe)$ with hydrosilanes under mild conditions [7]. In terms of reactions and mechanisms concerning the activation of silanes at triruthenium clusters, an early report by Süss-Fink and coworkers stands out. There the reversible reaction of $Ru_3(CO)_{11}(\mu\text{-}H)^-$ with two molecules of $HSiR_3$ was shown to furnish the novel clusters $Ru_3(CO)_{10}(SiR_3)_2(\mu\text{-}H)^-$, which exhibit catalytic activity in hydrosilylation [8]. Cabeza et al. investigated the reactivity of the face-capped clusters $Ru_3(CO)_9(\mu_3\text{-}\eta^3\text{-ampy})(\mu\text{-}H)$ and $Ru_3(CO)_8(PPh_3)(\mu_3\text{-}\eta^3\text{-ampy})(\mu\text{-}H)$ (Hampy = 2-amino-6-methylpyridine) and the edge-bridged cluster $Ru_3(CO)_7(\mu\text{-}CO)(\mu\text{-}C_4H_4N_2)$ ($C_4H_4N_2$ = pyridazine) with a wide range of tertiary silanes and obtained hydridosilyl derivatives without cluster fragmentation upon oxidative addition of Si–H bonds [9–11]. Nagashima and coworkers reported silyl complexes $Ru_3(CO)_6(\mu_3\text{-}\eta^2\text{:}\eta^3\text{:}\eta^5\text{-acenaphthylene})(SiR_3)(\mu\text{-}H)$ from the reactions of $Ru_3(CO)_7(\mu_3\text{-}\eta^2\text{:}\eta^3\text{:}\eta^5\text{-acenaphthylene})$ with trialkyl silanes [12]. It has been reported that reaction of the triruthenium cluster $Ru_3(CO)_7(\mu_3\text{-}\eta^5\text{:}\eta^5\text{-4,6,8-trimethylazulene})$ with $PhMe_2SiH$ resulted in the oxidative addition of Si–H bond, followed by the hydrogenation of one of the carbon–carbon double bonds in the azulene ligand to form the 46-electron cluster $Ru_3(CO)_6(\mu_2\text{-}\eta^3\text{:}\eta^5\text{-4,5-dihydro-4,6,8-trimethylazulene})(PhMe_2Si)(\mu\text{-}H)$ [13].

Adams et al. reported two silyl-containing pentaruthenium compounds, $Ru_5(CO)_{14}(SiEt_3)(\mu_5\text{-}C)(\mu\text{-}H)$ and $Ru_5(CO)_{15}(SiEt_3)(\mu_5\text{-}C)(\mu\text{-}H)$, from the oxidative addition of triethylsilane to $Ru_5(CO)_{15}(\mu_5\text{-}C)$ in the presence of UV–vis irradiation [14]. Finally, success in the oxidative addition of silanes to triosmium clusters has been achieved using the reactive clusters $Os_3(CO)_{10}(NCMe)_2$ [15,16] and the 46-electron dihydride cluster $Os_3(CO)_{10}(\mu\text{-}H)_2$ [17,18].

Cluster fragmentation following Si–H bond activation may be suppressed by edge-bridging ligands that reinforce the cluster framework. We have previously found that the oxidative addition of $R_3SiH$ (R = Ph, Et) to the unsaturated cluster $Os_3\{\mu_3\text{-}Ph_2PCH_2PPh(C_6H_4)\}(CO)_8(\mu\text{-}H)$ gives rise to $Os_3(CO)_9(\mu\text{-dppm})(SiR_3)(\mu\text{-}H)$ and $Os_3(CO)_7\{\mu_3\text{-}PPh_2CH_2PPh(C_6H_4)\}(SiR_3)(\mu\text{-}H)_2$ (R = Ph, Et) in which no cluster fragmentation has occurred [19]. The former products are also produced in the reaction of the parent cluster $Os_3(CO)_{10}(\mu\text{-dppm})$ with $R_3SiH$ (R = Ph, Et) at elevated temperatures [19]. Kira and co-workers reported that the reaction of $Ru_3(CO)_{10}(\mu\text{-dppm})$ (**1**) with $p\text{-tol}_2SiH_2$ proceeds with cluster fragmentation to afford the dinuclear complexes $Ru_2(CO)_6(\mu\text{-dppm})(\mu\text{-Sitol}_2)$ and $Ru_2(CO)_5(Sitol_2H)(\mu\text{-dppm})(\mu\text{-}\eta^2\text{-HSitol}_2)$ [20]; the latter was converted to the μ-silane complex $\{Ru(CO)_2(SiTol_2H)\}_2(\mu\text{-dppm})(\mu\text{-}\eta^2\text{:}\eta^2\text{-}H_2Sitol_2)_2$ upon further reaction with $p\text{-tol}_2SiH_2$ under photochemical conditions, as summarized in Scheme 1.

Although the reactivity of the dppm-bridged triruthenium cluster **2** has extensively been investigated [21–23], few studies have hitherto been published involving the dppf analog $Ru_3(CO)_{10}(\mu\text{-dppf})$ (**1**) [24,25]. We have recently explored the reactivity of the $P(C_4H_3E)_3$ (E = S, O) substituted derivatives of both **1** and **2**, and find that the thermolytic behavior of the dppm complexes $Ru_3(CO)_9(\mu\text{-dppm})\{P(C_4H_3S)_3\}$ and $Ru_3(CO)_9(\mu\text{-dppm})\{P(C_4H_3O)_3\}$ is significantly different from the corresponding dppf clusters $Ru_3(CO)_9(\mu\text{-dppf})\{P(C_4H_3S)_3\}$ and $Ru_3(CO)_9(\mu\text{-dppf})\{P(C_4H_3O)_3\}$. The former clusters undergo carbon–hydrogen and carbon–phosphorus bond scission under mild conditions (40 °C) to afford thiophyne and furyne complexes, respectively [23], whereas the latter clusters undergo ring cyclometalation, but only under forcing conditions (100 °C) [25]. With the above reactivity differences in mind, coupled with our interest in cluster-promoted substrate activation, we turned our attention toward the comparative study of the reactivity of diphosphine-tethered clusters $Ru_3(CO)_{10}(\mu\text{-dppf})$ (**1**), $Ru_3(CO)_{10}(\mu\text{-dppm})$ (**2**) and $Ru_3(CO)_9\{\mu_3\text{-}PPhCH_2PPh(C_6H_4)\}$ (**3**) with silanes.

## 2. Experimental section

### 2.1. General remarks

Unless otherwise noted, all reactions were carried out under a dry nitrogen atmosphere using standard Schlenk techniques. Reagent grade solvents were dried using appropriate drying agents and distilled prior to use by standard methods. $Ph_3SiH$, $Ph_2SiH_2$ and $Et_3SiH$ were purchased from Aldrich and used as received. The compounds $Ru_3(CO)_{10}(\mu\text{-dppf})$ (**1**) [26], $Ru_3(CO)_{10}(\mu\text{-dppm})$ (**2**) [27], and $Ru_3(CO)_9\{\mu_3\text{-}PPhCH_2PPh(C_6H_4)\}$ (**3**) [22a] were prepared according to published procedures. IR spectra were recorded on a Shimadzu FTIR 8101 spectrophotometer, and all NMR spectra were recorded on Varian Unity plus 400 spectrometers ($^1H$ NMR 400 MHz; $^{31}P$ NMR 162 MHz). All chemical shifts are reported in δ units and are referenced to the residual protons of the deuterated solvents ($^1H$) and to external $H_3PO_4$ ($^{31}P$). Elemental analyses were performed by the Microanalytical Laboratories of the Wazed Miah Science Research Centre at Jahangirnagar University. Product separations were performed by TLC in air on 0.5 mm silica gel ($HF_{254}$-type 60, E. Merck, Germany) glass plates.

### 2.2. Reaction of $Ru_3(CO)_{10}$(μ-dppf (**1**) with triphenylsilane

A dichloromethane solution (25 mL) of **1** (50 mg, 0.044 mmol) and $Ph_3SiH$ (24 mg, 0.088 mmol) was stirred at room temperature for 3 h, during which time the color changed from orange to deep red. The solvent was removed under reduced pressure and the residue chromatographed by TLC on silica gel. Elution with hexane/$CH_2Cl_2$ (7:3, v/v) developed one major and one very minor band. The major band afforded $Ru_3(CO)_9$(μ-dppf)($SiPh_3$)(μ-H) (**4**) (36 mg, 60%) as red crystals from hexane/$CH_2Cl_2$. Anal. Calcd. for $C_{61}H_{44}FeO_9P_2Ru_3Si$: C, 53.48; H, 3.24. Found: C, 53.65; H, 3.35%. IR (νCO, $CH_2Cl_2$): 2076 w, 2041 m, 2004 vs, 1967 sh $cm^{-1}$. $^1H$ NMR ($CDCl_3$) 298 K: δ 7.74 (m, 6H), 7.45 (m, 20H), 7.26 (m, 9H), 4.44 (s, 4H), 4.16 (br, s, 4H), −16.53 (t, 1H, $J = 9.8$ Hz); 218 K: δ 7.55 (m, 22H), 7.29 (m, 8H), 7.25 (m, 3H), 7.09 (m, 2H), 4.60 (s, 1H), 4.53 (s, 1H), 4.50 (s, 1H), 4.37 (s, 2H), 4.28 (s, 1H), 4.00 (s, 1H), 3.74 (s, 1H), −16.68 (t, 1H, $J = 9.8$ Hz). $^{31}P\{^1H\}$ NMR ($CDCl_3$) 298 K: δ 20.6 (s, 2P); 218 K: δ 20.5 (s, 1P), 21.4 (s, 1P). FAB-MS: *m*/*z* 1371.

### 2.3. Reaction of **1** with triethylsilane

A THF solution (30 mL) of **1** (50 mg, 0.044 mmol) and $Et_3SiH$ (10 mg, 0.088 mmol) was heated to reflux for 1 h, during which time the color changed from orange to red. The solvent was removed under reduced pressure and the residue chromatographed by TLC on silica gel. Elution with hexane/$CH_2Cl_2$ (7:3, v/v) developed one major and two minor bands. The major band afforded $Ru_3(CO)_9$(μ-dppf)($SiEt_3$)(μ-H) (**5**) as red crystals after recrystallization from hexane/$CH_2Cl_2$ at 4 °C (24 mg, 45%). Anal. Calcd. for $C_{49}H_{44}FeO_9P_2Ru_3Si$: C, 48.01; H, 3.62. Found: C, 48.25; H, 3.79. IR (νCO, $CH_2Cl_2$): 2073 w, 2036 m, 1998 vs, 1962 sh $cm^{-1}$. $^1H$ NMR ($CDCl_3$) 293 K: δ 7.47 (m, 20H), 4.24 (s, 4H), 4.11 (br, s, 4H), 0.99 (t, 9H, $J = 8.0$ Hz), 0.62 (q, 6H, $J = 8.0$ Hz) −16.63 (t, 1H, $J = 10.4$ Hz). $^{31}P\{^1H\}$NMR ($CDCl_3$): δ 28.3 (br, s, 2P). FAB MS: *m*/*z* 1227.

### 2.4. Reaction of **1** with diphenylsilane

A $CH_2Cl_2$ solution (15 mL) of $Me_3NO$ (4 mg, 0.053 mmol) was added dropwise to a $CH_2Cl_2$ solution (20 mL) of **1** (50 mg, 0.044 mmol) and $Ph_2SiH_2$ (16 mg, 0.088 mmol) over a period of 30 min, and the resulting solution was stirred for an additional 1 h. Similar work up and chromatographic separation, as described above, developed one major and two very minor bands. The major band gave $Ru_3(CO)_9$(μ-dppf)($SiPh_2H$)(μ-H) (**6**) (30 mg, 53% yield) after recrystallization from hexane/$CH_2Cl_2$ at 4 °C. Anal. Calcd for $C_{55}H_{40}FeO_9P_2Ru_3Si$: C, 51.05; H, 3.12. Found: C, 51.25; H, 3.23. IR (νCO, $CH_2Cl_2$): 2077 w, 2042 m, 2003 vs, 1967 sh $cm^{-1}$. $^1H$ NMR ($CDCl_3$) 298 K: δ 7.82 (m, 4H), 7.46 (m, 22H), 7.32 (m, 2H), 7.24 (m, 2H), 5.70 (s, 1H), 4.32 (s, 4H), 4.12 (br, s, 4H), −16.68 (t, 1H, $J = 10.4$ Hz); 243 K: δ 7.83 (m, 4H), 7.57 (m, 20H), 7.33 (m, 3H), 7.25 (m, 3H), 5.63 (s, 1H), 4.39 (s, 4H), 4.27 (s, 1H), 4.14 (s, 1H) 3.78 (s, 1H) 3.72 (s, 1H), −16.82 (dd, 1H, $J = 10.0, 10.8$ Hz). $^{31}P\{^1H\}$NMR ($CDCl_3$) 298 K: δ 21.1 (br, s, 1P), 19.1 (br, s, 1P); 243 K: δ 21.0 (s, 1P), 19.0 (s, 1P). FAB MS: *m*/*z* 1295.

### 2.5. Reaction of $Ru_3(CO)_{10}$(μ-dppm) (**2**) with triphenylsilane

To a $CH_2Cl_2$ solution (30 mL) of **2** (100 mg, 0.103 mmol) and $Ph_3SiH$ (54 mg, 0.207 mmol) was added dropwise a $CH_2Cl_2$ solution (15 mL) of $Me_3NO$ (12 mg, 0.16 mmol) over a period of 1 h, during which time the color changed from orange to deep red. The solvent was removed under reduced pressure and the residue chromatographed by TLC on silica gel. Elution with hexane/$CH_2Cl_2$ (3:1, v/v) developed three bands. The first band was unreacted **2** (5 mg), the second band afforded $Ru_3(CO)_9$(μ-dppm)($SiPh_3$)(μ-H) (**7**) (65 mg, 40%), as red crystals after recrystallization from hexane/$CH_2Cl_2$ in the presence of $Ph_3SiH$ (1 drop) at 4 °C, and the third band yielded $Ru_3$(μ$_3$-O)(μ-dppm)$(CO)_6(SiPh_3)$(μ-H)$_3$ (**8**) (9 mg, 15%), which was isolated as pale yellow crystals after recrystallization from hexane/$CH_2Cl_2$ at 4 °C. Analytical and spectroscopic data for **7**: Anal. Calcd for $C_{52}H_{38}O_9P_2Ru_3Si$: C, 52.04; H, 3.19. Found: C, 52.25; H, 3.45%. IR (νCO, $CH_2Cl_2$): 2076 w, 2044 s, 2003 s, 1995 sh $cm^{-1}$. $^1H$ NMR ($CD_2Cl_2$): δ 7.31 (m, 9H), 7.41 (m, 11H), 7.55 (m, 15H), 4.47 (t, 2H, $J = 10.8$ Hz), −18.10 (d, 1H, $J = 32.0$ Hz). $^{31}P\{^1H\}$ NMR ($CD_2Cl_2$): δ 10.4 (d, $J = 45.3$ Hz), 8.9 (d, $J = 45.3$ Hz). FAB MS: *m*/*z* 1201. Spectroscopic data for **8**: Anal. Calcd for $C_{49}H_{40}O_7P_2Ru_3Si$: C, 51.90; H, 3.56. Found: C, 52.05; H, 3.62%. IR (νCO, $CH_2Cl_2$): 2040 vs, 2012 m, 1990 s, 1946 m $cm^{-1}$. $^1H$ NMR ($CD_2Cl_2$): δ 7.81 (m, 8H), 7.61 (m, 4H), 7.41 (m, 16H), 7.05 (m, 2H), 6.91 (m, 5H), 3.51 (m, 1H), 3.04 (m, 1H), −16.08 (br, s, 1H), −14.56 (d, 1H, $J = 60.0$ Hz), −11.75 (d, 1H, $J = 74.4$ Hz). $^{31}P\{^1H\}$ NMR ($CD_2Cl_2$): δ 27.9 (d, $J = 61.0$ Hz), 24.1 (d, $J = 61.0$ Hz). FAB MS: *m*/*z* 1133. Similar reactions of **2** with $Et_3SiH$ or $Ph_2SiH_2$ afforded only intractable materials.

### 2.6. Reaction of **7** with water

To a $CH_2Cl_2$ solution of 7 (10 mg, 0.008 mmol) was added one drop of water, followed by stirring for 3 h at room temperature. The solvent was removed under reduced pressure and the residue chromatographed by TLC on silica gel. Elution with hexane/$CH_2Cl_2$ (3:1, v/v) developed three bands which afforded, in order of elution, **1** (2 mg, 25%), unreacted **7** (5 mg, 50%) and **8** (1.5 mg, 16%).

### 2.7. Reaction of $Ru_3(CO)_9\{\mu_3$-$PPhCH_2PPh(C_6H_4)\}$ (**3**) with triphenylsilane

Triphenylsilane (54 mg, 0.22 mmol) was added to a THF solution (25 mL) of **3** (80 mg, 0.093 mmol) and the reaction mixture refluxed for 3.5 h, during which the color changed from orange to red. The solvent was removed under reduced pressure and the residue chromatographed by TLC on silica gel. Elution with hexane/$CH_2Cl_2$, (4:1, v/v) afforded $Ru_3$(μ-CO)$(CO)_7\{\mu_3$-$PPhCH_2PPh(C_6H_4)\}(SiPh_3)$(μ-H) (**9**) (45 mg, 71%) as pale yellow crystals from hexane/$CH_2Cl_2$ at 4 °C. Anal. Calcd for $C_{45}H_{32}O_8P_2Ru_3Si$: C, 49.41; H, 2.95. Found: C, 49.65; H, 3.05. IR (νCO, $CH_2Cl_2$): 2079 vs, 2044 vs, 2027 s, 2015 m, 1975 m, 1869 w $cm^{-1}$. $^1H$ NMR ($CDCl_3$): δ 7.83 (m, 1H), 7.55 (m, 5H), 7.32 (m, 10H), 7.24 (m, 10H), 6.98 (m, 1H), 6.71 (m, 1H), 6.14 (m, 1H), 4.43 (m, 1H), 3.75 (m, 1H), −16.10 (m, 1H). $^{31}P\{^1H\}$NMR ($CDCl_3$): δ 88.6 (d, $J = 81.9$ Hz), −0.7 (d, $J = 81.9$ Hz).

### 2.8. Reaction of **3** with triethylsilane

A THF solution (50 mL) of **3** (0.10 g, 0.12 mmol) and triethylsilane (68 mg, 0.58 mmol) was heated to reflux for 30 min, during which time the color changed from orange to red. After removal of the solvent under reduced pressure, the residue was purified by TLC on silica gel. Elution with hexane/$CH_2Cl_2$ (7:3, v/v) developed two bands. The major band afforded $Ru_3$(μ-CO)$(CO)_7\{\mu_3$-$PPhCH_2PPh(C_6H_4)\}(SiEt_3)$(μ-H) (**10**) in 60% yield (34 mg) as red crystals after recrystallization from hexane/$CH_2Cl_2$ at 4 °C. Anal. Calcd. for $C_{33}H_{32}O_8P_2Ru_3Si$: C, 41.73; H, 3.40. Found: C, 42.05; H, 3.65%. IR (νCO, $CH_2Cl_2$): 2077 vs, 2040 vs, 2021 vs, 2008 m 1970 m, 1863 w $cm^{-1}$. $^1H$ NMR ($CDCl_3$): δ 7.86 (m, 1H), 7.70 (m, 3H), 7.62 (m, 2H), 7.37 (m, 5H), 7.02 (m, 1H), 6.75 (m, 1H), 6.22 (m, 1H), 3.77 (m, 1H), 3.13 (m, 1H), 0.91 (m, 6H), 0.83 (m, 9H), −16.50 (m, 1H). $^{31}P\{^1H\}$NMR ($CDCl_3$): δ 80.9 (d, $J = 82.5$ Hz), −0.09 (d, $J = 82.5$ Hz). The minor band was too small for complete characterization.

**Table 1**
Crystallographic data and structure refinement for **4**, **8** and **9**.

| Compound | **4** | **8** | **9** |
|---|---|---|---|
| Empirical formula | $C_{61}H_{44}FeO_9P_2Ru_3Si$ | $C_{49}H_{40}O_7P_2Ru_3Si$ | $C_{45.13}H_{32}Cl_{0.50}O_8P_2Ru_3Si$ |
| Formula weight | 1370.05 | 1134.05 | 1113.17 |
| Temperature (K) | 150(2) | 293(2) | 100(2) |
| Wavelength (Å) | 0.71073 | 0.71073 | 0.71073 |
| Cryst system | Triclinic | Monoclinic | Monoclinic |
| Space group | $P\bar{1}$ | $P\,2_1/n$ | $C2/c$ |
| $a$ (Å) | 11.470(3) | 11.5517(9) | 14.554(3) |
| $b$ (Å) | 12.921(4) | 14.8235(12) | 11.1260(7) |
| $c$ (Å) | 20.603(6) | 27.905(2) | 19.526(12) |
| $\alpha$ (°) | 89.139(5) | 90 | 90 |
| $\beta$ (°) | 82.770(6) | 99.8050(10) | 96.391(2) |
| $\gamma$ (°) | 69.517(5) | 90 | 90 |
| Volume (Å$^3$) | 2836.3(15) | 4708.5(6) | 8971.4(10) |
| $Z$ | 2 | 4 | 8 |
| $D_{calc}$ (Mg m$^{-3}$) | 1.604 | 1.600 | 1.648 |
| $\mu$ (Mo K$\alpha$) (mm$^{-1}$) | 1.168 | 1.093 | 1.176 |
| $F$(000) | 1368 | 2264 | 4410 |
| Crystal size (mm) | 0.22 × 0.16 × 0.12 | 0.44 × 0.26 × 0.25 | 0.47 × 0.32 × 0.18 |
| $\theta$ range (°) | 2.57–28.55 | 1.56–28.26 | 1.90–28.39 |
| Limiting indices | $-15 \le h \le 14$, $-16 \le k \le 17$, $-26 \le l \le 27$ | $-15 \le h \le 15$, $-19 \le k \le 19$, $-35 \le l \le 36$ | $-55 \le h \le 55$, $-14 \le k \le 14$, $-26 \le l \le 26$ |
| Reflections collected | 23,891 | 41,078 | 60,596 |
| Independent reflections ($R_{int}$) | 12,757 (0.0952) | 11,244 (0.0213) | 11,197 (0.0304) |
| Max. and min. transmission | 0.8726 and 0.7832 | 0.7680 and 0.6443 | 0.8162 and 0.6079 |
| Data/restraints/parameters | 12,757/0/685 | 11,244/0/571 | 11,197/9/335 |
| Goodness of fit on $F^2$ | 0.830 | 0.819 | 1.109 |
| Final $R$ indices [$F^2 > 2\sigma$] | $R_1 = 0.0773$, $wR_2 = 0.1784$ | $R_1 = 0.0300$, $wR_2 = 0.0782$ | $R_1 = 0.0534$, $wR_2 = 0.1663$ |
| $R$ indices (all data) | $R_1 = 0.1688$, $wR_2 = 0.2165$ | $R_1 = 0.0355$, $wR_2 = 0.0827$ | $R_1 = 0.0560$, $wR_2 = 0.1694$ |
| Largest difference in peak and hole (e Å$^{-3}$) | 2.936 and −1.781 | 0.829 and −0.355 | 3.476 and −1.903 |

Crystallographic data and structure refinement for **10** and **11**

| Compound | **10** | **11** |
|---|---|---|
| Empirical formula | $C_{33}H_{31}O_8P_2Ru_3Si$ | $C_{39}H_{28}O_8P_2Ru_3Si$ |
| Formula weight | 948.82 | 1017.85 |
| Temperature (K) | 100(2) | 150(2) |
| Wavelength (Å) | 0.71073 | 0.71073 |
| Cryst system | Orthorhombic | Monoclinic |
| Space group | Pbca | $P\,2_1/n$ |
| $a$ (Å) | 17.648(5) | 13.079(3) |
| $b$ (Å) | 18.641(5) | 12.632(3) |
| $c$ (Å) | 22.144(6) | 23.323(5) |
| $\beta$ (°) | 90 | 104.921(4) |
| Volume (Å$^3$) | 7285(3) | 3723.5(14) |
| $Z$ | 8 | 4 |
| $D_{calc}$ (Mg m$^{-3}$) | 1.730 | 1.816 |
| $\mu$ (Mo K$\alpha$) (mm$^{-1}$) | 1.396 | 1.372 |
| $F$(000) | 3752 | 2008 |
| Crystal size (mm) | 0.38 × 0.30 × 0.11 | 0.46 × 0.20 × 0.16 |
| $\theta$ range (°) | 1.84–31.98 | 2.64–28.32 |
| Limiting indices | $0 \le h \le 26$, $0 \le k \le 27$, $0 \le l \le 32$ | $-17 \le h \le 17$, $-16 \le k \le 16$, $-30 \le l \le 29$ |
| Reflections collected | 12,200 | 29,971 |
| Independent reflections ($R_{int}$) | 12,200 (0.0535) | 8649 (0.0509) |
| Max. and min. transmission | 0.8616 and 0.6191 | 0.8103 and 0.5709 |
| Data/restraints/parameters | 12,200/12/458 | 8649/0/490 |
| Goodness of fit on $F^2$ | 1.162 | 0.898 |
| Final $R$ indices [$F^2 > 2\sigma$] | $R_1 = 0.0500$, $wR_2 = 0.1087$ | $R_1 = 0.0324$, $wR_2 = 0.0614$ |
| R indices (all data) | $R_1 = 0.0637$, $wR_2 = 0.1133$ | $R_1 = 0.0538$, $wR_2 = 0.0639$ |
| Largest difference in peak and hole (e Å$^{-3}$) | 1.713 and −0.958 | 0.715 and −0.651 |

### 2.9. Reaction of **3** with diphenylsilane

Diphenylsilane (22 mg, 0.12 mmol) was added to a THF solution (15 mL) of **3** (50 mg, 0.058 mmol) and the reaction mixture was refluxed for 3.5 h. The solvent was removed under reduced pressure and the residue chromatographed by TLC on silica gel. Elution with cyclohexane/$CH_2Cl_2$, (4:1, v/v) afforded $Ru_3(\mu\text{-}CO)(CO)_7\{\mu_3\text{-}PPhCH_2PPh(C_6H_4)\}(SiPh_2H)(\mu\text{-}H)$ (**11**) (40 mg, 66%) as pale yellow crystals from hexane/$CH_2Cl_2$ at 4 °C. Anal. Calcd. for $C_{39}H_{28}O_8P_2Ru_3Si$: C, 46.02; H, 2.77. Found: C, 46.26; H, 2.95%. IR ($\nu$CO, $CH_2Cl_2$): 2079 vs, 2044 vs, 2028 vs, 2014 sh, 1975 w, 1867 w cm$^{-1}$. $^1$H NMR ($CD_2Cl_2$): $\delta$ 7.92 (m, 1H), 7.53 (m, 9H), 7.35 (m, 8H), 7.17 (m, 1H), 7.06 (m, 3H), 6.75 (m, 1H), 6.19 (m, 1H), 5.75 (d, 1H, $J$ = 4.0 Hz), 2.85 (m, 1H), 2.56 (m, 1H), −16.39 (m, 1H). $^{31}$P {$^1$H}NMR ($CD_2Cl_2$): $\delta$ 89.7 (d, $J$ = 78.3 Hz), −1.5 (d, $J$ = 78.3 Hz).

### 2.10. Crystal structure determinations

Single crystals of **4**, **8**, **10** and **11** were mounted on fibers and diffraction data collected on a Bruker SMART APEX CCD diffractometer using Mo K$\alpha$ radiation ($\lambda$ = 0.71073 Å). Data reduction and integration were carried out with SAINT+, and absorption

corrections were applied using the program SADABS [28]. The structures were solved by direct methods and developed using alternating cycles of least-squares refinement and difference Fourier synthesis. All non-hydrogen atoms were refined anisotropically. Hydrogen atoms, except those directly bonded to ruthenium, were placed in the calculated positions and their thermal parameters linked to those of the atoms to which they were attached (riding model). We were unable to locate the hydride on cluster **4** but all three hydrides on cluster **8** were located from the difference map. The quality of crystal of **4** used for the diffraction data had a large mosaic spread, so even after final refinement the R values are high. Several attempts have been made to grow good quality crystals but were unsuccessful. The SHELXTL PLUS V6.10 program package was used for structure solution and refinement [29]. Final difference maps did not show any residual electron density of stereochemical significance. The details of the data collection and structure refinement are given in Table 1.

A suitable crystal of **9** was coated with Paratone-N oil, suspended in a small fiber loop, and placed in a cooled nitrogen gas stream at 100 K on a Bruker D8 SMART APEX CCD sealed tube diffractometer with graphite-monochromated Mo-Kα (0.71073 Å) radiation. All data were measured using a series of combinations of phi and omega scans with 10 s frame exposures and 0.3 frame widths. Data collection, indexing, and initial cell refinements were all carried out using SMART software [30]. Frame integration and final cell refinements were done using SAINT software [31]. The final cell parameters were determined from least-squares refinement. The SADABS [32] program was used to carry out absorption corrections. The structures were solved using direct methods and difference Fourier techniques (SHELXTL, V6.12) [33]. Hydrogen atoms were placed in their expected chemical position using the HFIX command and were included in the final cycles of least squares with isotropic Uij's related to the atoms ridden on. The hydrides were positioned by using the XHYDEX program in the WinGX suite of programs [34]. All non-hydrogen atoms were refined anisotropically. Scattering factors and anomalous dispersion corrections are taken from International Tables for X-ray Crystallography [35]. One of the phenyl rings in **9** was disordered and no attempt has been made to model this. Structure solution, refinement, graphics, and generation of publication materials were performed by using SHELXTL, V6.12 software. Additional details of data collection and structure refinement are given in Table 1.

### 2.11. Computational details and methodology

The DFT calculations were conducted using Morokuma's ONIOM method [36], as implemented by the Gaussian 09 program software [37]. The different species were optimized via a two-level approach with the phenyl groups of the silane reagent $Ph_3SiH$ and the $Ph_3Si$ and dppf ligands treated as the lower of the two levels; the atoms in all other compounds were optimized by *ab initio* DFT methods. For those species analyzed within the two-level treatment, we employed an ONIOM method that was defined by a B3LYP/PM6 composition. The phenyl groups (low level) were treated at the semiempirical PM6 level of theory, while the remaining atoms (high level) were treated within the B3LYP framework. With respect to the high-level treatment of atoms, the ruthenium atoms were described by Stuttgart–Dresden effective core potentials (ecp) and SDD basis set, while a 6-31G(d′) basis set was employed for the remaining atoms. All reported geometries were fully optimized and evaluated for the correct number of imaginary frequencies through calculation of the vibrational frequencies, using the analytical Hessian. Zero imaginary frequencies (positive eigenvalues) represent ground-state structures, while a species with an imaginary frequency (negative eigenvalue) designates a transition state. The transition states on the potential energy surface were evaluated by IRC calculations in order to confirm the connecting reactant and product species. The computed frequencies were used to make zero-point and thermal corrections to the electronic energies, and the reported potential energies are quoted in kcal/mol relative to the starting cluster $Ru_3(CO)_{10}(dppf)$ (**A**) and $Ph_3SiH$ (**C**). The geometry-optimized structures depicted in Figs. 1 and 3 have been drawn with the *JIMP2* molecular visualization and manipulation program [38].

## 3. Results and discussion

### 3.1. Oxidative addition of silanes to $Ru_3(CO)_{10}(\mu$-dppf) (**1**)

Reactions of **1** with excess $Ph_3SiH$ and $Ph_2SiH_2$ at room temperature afforded $Ru_3(CO)_9(\mu$-dppf)$(SiPh_3)(\mu$-H) (**4**) (60% yield) and $Ru_3(CO)_9(\mu$-dppf)$(SiPh_2H)(\mu$-H) (**6**) (53% yield), respectively (Scheme 2). However, compound **1** does not react with $Et_3SiH$ at room temperature but does react at 68 °C to give $(\mu$-H)$Ru_3(CO)_9(\mu$-dppf)$(SiEt_3)$ (**5**) (45% yield). Compounds **4**–**6** are formed by

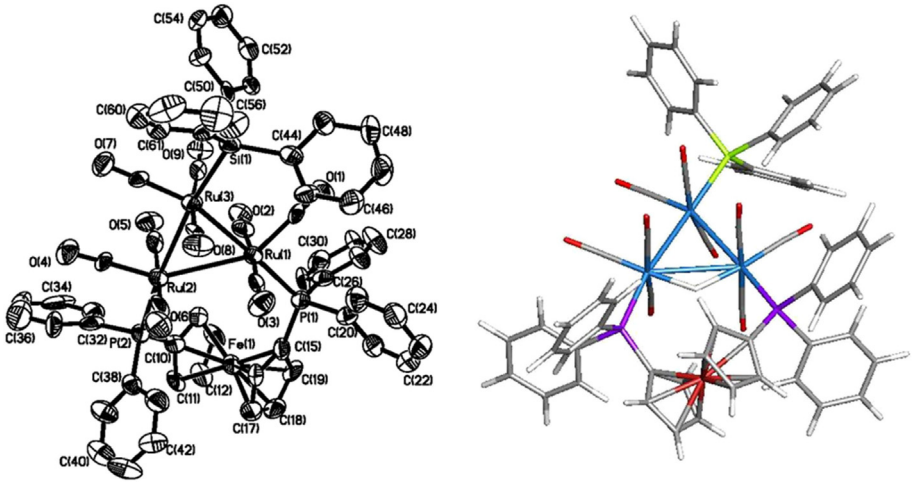


**Fig. 1.** ORTEP drawing of the molecular structure of $Ru_3(CO)_9(SiPh_3)(\mu$-dppf)$(\mu$-H) (**4**) (left) and DFT-optimized structure **G** (right). Selected X-ray diffraction data [bond lengths (Å) and angles (°)] for **4**: Ru(1)–Ru(2) 3.033(1), Ru(2)–Ru(3) 2.868(1), Ru(1)–Ru(3) 2.866(1), Ru(1)–P(1) 2.323(3), Ru(2)–P(2) 2.327(3), Ru(3)–Si(1) 2.417(3), Ru(1)–Ru(2)–Ru(3) 58.04(3), Ru(1)–Ru(3)–Ru(2) 63.86(3), Ru(3)–Ru(1)–Ru(2) 58.10(3), P(2)–Ru(2)–Ru(3) 171.47(8), P(2)–Ru(2)–Ru(1) 114.80(8), P(1)–Ru(1)–Ru(3) 174.85(9), P(1)–Ru(1)–Ru(2) 120.69(8), Si(1)–Ru(3)–Ru(1) 110.63(8), Si(1)–Ru(3)–Ru(2) 170.57(8), P(1)–C(15)–Fe(1) 132.7(6), P(2)–C(10)–Fe(1) 131.2(6).

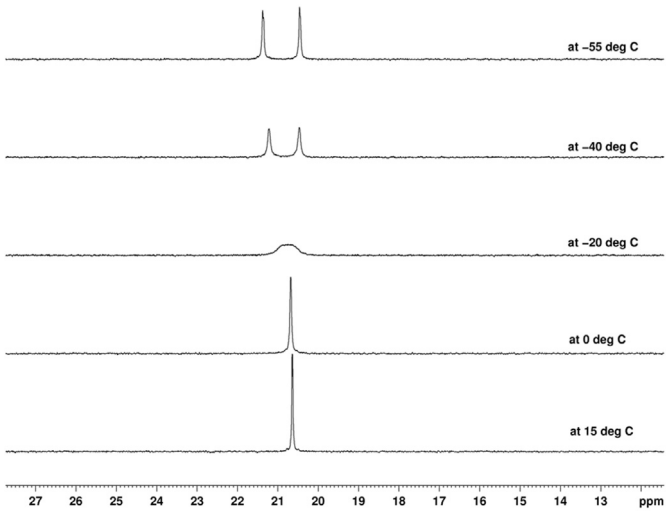


**Fig. 2.** $^{31}P\{^{1}H\}$ NMR spectra of $Ru_3(CO)_9(SiPh_3)(\mu\text{-dppf})(\mu\text{-H})$ **4**.

dissociation of a CO from **1**, followed by oxidative addition of a Si–H bond. Characterization of **4**–**6** has been made by elemental analysis, mass spectrometry, IR and NMR ($^{1}H$ and $^{31}P\{^{1}H\}$) spectroscopy and by single crystal X-ray diffraction analysis in the case of **4**.

The molecular structure of **4** is shown in Fig. 1, and the caption contains selected bond distances and angles. The structure consists of a triangular array of ruthenium atoms with two short [Ru(2)–Ru(3) 2.868(1), Ru(1)–Ru(3) 2.866(1) Å] and one comparatively long [Ru(1)–Ru(2) 3.033(1) Å] ruthenium–ruthenium interactions, the latter being the metal–metal vector spanned by the dppf and hydride ligands. The disposition of the hydride along the Ru(1)–Ru(2) edge is confirmed by NMR spectroscopy and DFT calculations (see below). This edge is much longer than the other two Ru–Ru bonds in **4** and is also longer than the corresponding dppf-bridged Ru–Ru bond in **1** [2.9284(5) Å] [39], as is typically found for metal–metal bonds that are bridged by a hydride ligand(s). Nine CO ligands are bound to the cluster, and each ruthenium atom has three CO ligands. The coordination geometry at each Ru atom is closely octahedral, with the hydride occupying one of the octahedral sites at the Ru(1) and Ru(2) centers. The unbridged Ru–Ru distances are very similar to those distances reported for **1** [2.8600(4) Å], while the two Ru–P distances are almost equal [Ru(1)–P(1) 2.323(3), Ru(2)–P(2) 2.327(3) Å] and compare favorably with the Ru–P distances [2.3503(8) Å] found in **1** [40]. In the crystal structure, the ferrocene moiety shows no adverse interactions with the triruthenium framework. The $SiPh_3$ moiety is bound to the Ru(3) atom at the sterically least crowded equatorial site in the cluster and the Ru–Si distance is 2.417(3) Å. The Ru–Si bond distance is similar to those found in related triruthenium clusters such as 2.441(3) Å, 2.450(2) Å in $Ru_3(CO)_{10}(SiEt_3)_2(\mu\text{-H})^-$ [8b]; 2.460(6) Å, 2.455(5) Å in $Ru_3(CO)_8(SiEt_3)_2(\mu\text{-}C_4H_4N_2)(\mu\text{-H})_2$ [10]; 2.435(4) Å in $Ru_3(CO)_8(SiEt_3)(\mu_3\text{-}HNC_6H_3Me)(\mu\text{-H})_2$ [9]. While the overall structure of **4** is similar to those complexes of the type $Ru_3(CO)_9(\mu\text{-diphosphine})(PR_3)$ [23,25,40,41], it is only the second example of a triruthenium cluster that possesses a bridging dppf ligand and one additional monodentate ligand within the coordination sphere of the cluster. The only other paradigm being $Ru_3(CO)_9(\mu\text{-dppf})(PFu_3)$, which was recently reported by us from the $Me_3NO$-induced decarbonylation reaction between $Ru_3(CO)_{10}(\mu\text{-dppf})$ and $PFu_3$ [25].

The bonding in **4** was also investigated by DFT calculations, and the geometry-optimized structure (**G**) is shown alongside the X-ray diffraction structure. The hydride ligand spans the dppf-bridged Ru–Ru vector and lies essentially in the plane defined by the three metals. The two non-bridged Ru–Ru vectors display a mean distance of 3.000 Å and the hydride-bridged Ru–Ru bond distance in **G** is computed as 3.205 Å. These distances and the disposition of the ligands about the cluster core in **G** are in concert with the solid-state structure.

Compounds **4**–**6** are fluxional in solution, as evidenced by their temperature-dependent $^{1}H$ and $^{31}P\{^{1}H\}$ NMR spectra, which have been probed for clusters **4** and **6**. As the three species exhibit similar behavior in solution, only the VT NMR of **4** will be discussed in detail (Fig. 2). At 15 °C, the $^{31}P\{^{1}H\}$ NMR spectrum exhibits a sharp signal at $\delta$ 20.6. On cooling to −20 °C, the signal becomes very broad and at −55 °C this signal separates into two sharp, equal intensity singlets at $\delta$ 21.4 and 20.5, showing that the fluxionality is fully arrested at this temperature. The slow-exchange spectrum reveals a $\Delta\nu$ of 149 Hz for these resonances, and in conjunction with the coalescence temperature of 248 K ($T_c$), we estimate a $\Delta G^{\neq}$ value of 11.2 kcal/mol for this equilibration process involving the two phosphine groups [42]. The $^{1}H$ NMR spectra also shed light on the fluxional process. At 15 °C, the cyclopentadienyl protons appear as two equal intensity singlets, one very broad singlet at $\delta$ 4.16 and another comparatively sharp singlet at $\delta$ 4.44. At 0 °C the broad singlet at $\delta$ 4.16 becomes barely indistinguishable from the base line and the other cyclopentadienyl resonance becomes broad. These signals separate into seven singlets at −55 °C, six of equal intensity that integrate for 1H each, with the remaining resonance integrating for 2H, confirming the arrested fluxionality. In terms of the bridging hydride, the hydride appears as a triplet at $\delta$ −16.53 at 15 °C. The observed splitting pattern indicates that the two phosphines are equally coupled to the bridging hydride. Apart from a slight high-field shift ($\delta$ −16.68) upon cooling to −55 °C, the hydride remains a well-defined binomial triplet. We interpret these temperature-dependent spectral changes to the conformational flexibility of the dppf ligand in **4**. The behavior of the dppf ligand in **4** is analogous to that found by us in the dppf-bridged cluster $Os_3(CO)_{10}(dppf)$ [26].

Compounds **5** and **6** exhibit spectroscopic properties similar to that of **4**. All three products exhibit four carbonyl absorptions bands in the carbonyl region of their IR spectrum, and the intensities and

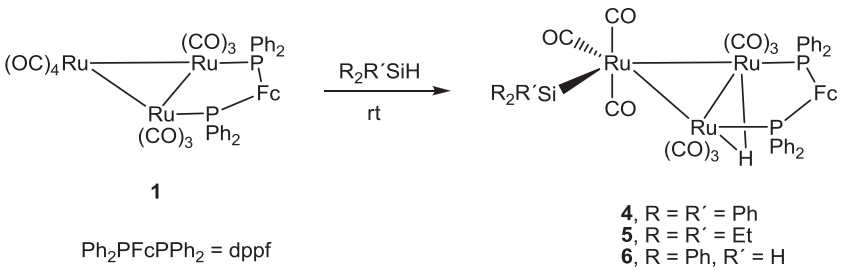


**1**

$Ph_2PFcPPh_2$ = dppf

**4**, R = R´ = Ph
**5**, R = R´ = Et
**6**, R = Ph, R´ = H

**Scheme 2.**

spectral patterns reinforce their isostructural nature. Each $^{31}P\{^{1}H\}$ NMR spectrum displays two singlets at low temperature, which confirms that the phosphorus atoms are nonequivalent in the limiting spectrum. The dynamic behavior of the cyclopentadienyl hydrogens and the phosphine groups in the $^{1}H$ and $^{31}P$ spectra of **5** and **6** indicates that the ancillary dppf is conformationally flexible. These data support a common, low-energy exchange process involving the diphosphine ligand in this genre of $Ru_3(CO)_9(\mu\text{-dppf})(SiR_3)(\mu\text{-H})$ clusters.

The reaction path responsible for the formation of **4** (species **G**) was examined computationally, starting from **1**. Figs. 3 and 4 show the pertinent geometry-optimized structures and the potential-energy profile leading to **G**. The optimized structure of **A** shows an excellent correspondence to the solid-state structure [39], including the pronounced $D_3$ twist in the axial CO groups. Silane activation is initiated by the site-selective loss of an axial CO in **A** to generate the unsaturated species **B** and free CO, which lie 33.0 kcal/mol above the parent cluster. The transition state **TSBCD** reveals that the oxidative addition of the silane occurs at the axial site originally occupied by the liberated CO, and the resulting product **D** contains axial $Ph_3Si$ and bridging hydride groups. A turnstile rotation of the groups at the $Ru(CO)_3(SiPh_3)$ center, which proceeds via **TSDE**, promotes the formation of the equatorial $Ph_3Si$ group and yields species **E**. The axial-to-equatorial migration of the $Ph_3Si$ group is thermodynamically favorably and **E** is 11.8 kcal/mol more stable than **D**. Migration of the edge-bridging hydride in **D** to an interstitial locus in **F** constitutes the penultimate step in the reaction. Continued transit of the hydride to the thermodynamically

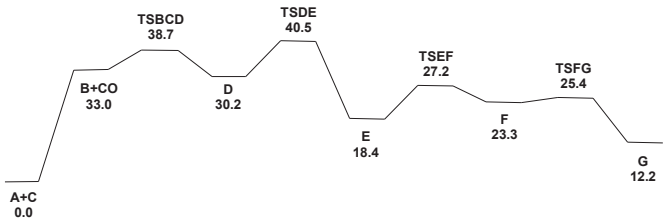


**Fig. 4.** Potential energy surface for the conversion of **A** to **G** in the presence of $Ph_3SiH$ (**C**). Energy values are $\Delta E$ in kcal/mol with respect to **A** and **C**.

preferred Ru–Ru edge that is tethered by the dppf ligand affords the final species **G**. While the formation of **G** and CO relative to **A** and $Ph_3SiH$ is uphill by 12.2 kcal/mol, the release of CO in the first step of the reaction is entropically favored, and this serves to drive the overall reaction to the experimentally observed silyl-hydride **G**.

### 3.2. Oxidative addition of H–Si bonds to $Ru_3(CO)_{10}(\mu\text{-dppm})$ (**2**)

With the aim of comparing the reactivity of the relatively rigid dppm analog **2** with that of more flexible dppf compound **1**, we have studied the reactions of **2** with silanes. Scheme 3 illustrates the course of these reactions. Compound **2** has been shown to exhibit significantly greater reactivity than the comparatively unreactive $Ru_3(CO)_{12}$, and the small-bite angle dppm ligand helps to maintain the integrity of the trinuclear cluster framework. In contrast to the reaction of **2** with $p\text{-tol}_2SiH_2$ which afforded

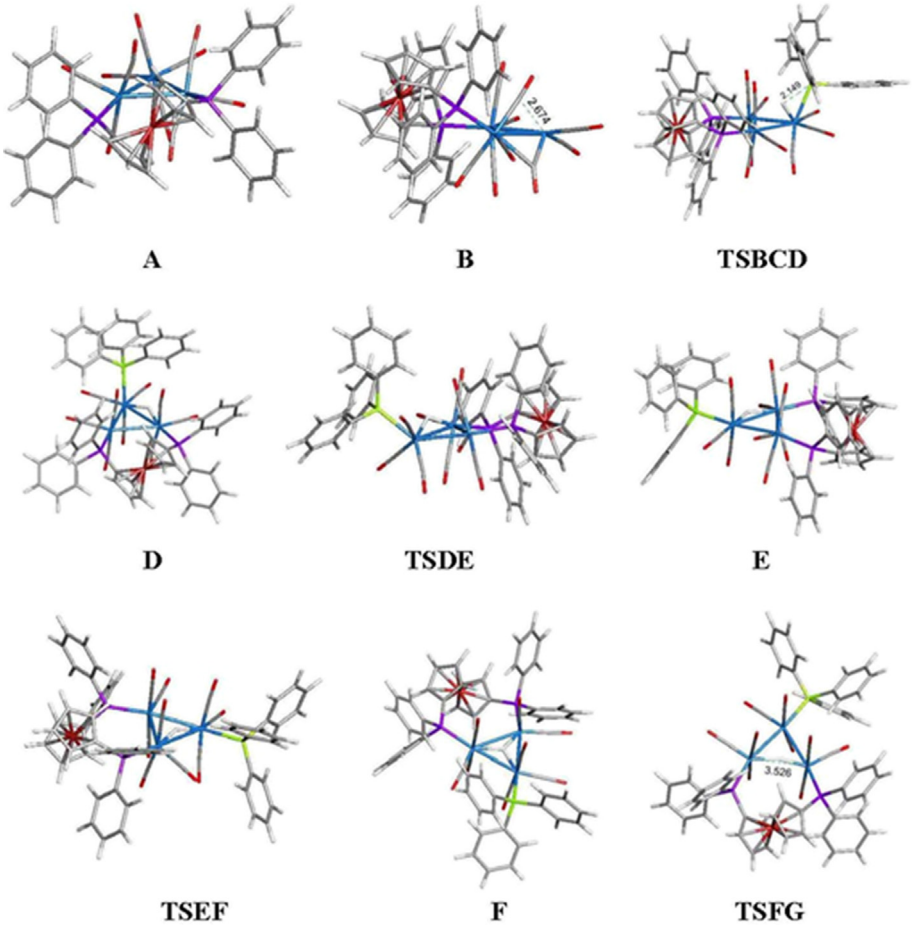


**Fig. 3.** B3LYP-optimized structures for the intermediates **A**–**F** and the corresponding transition states. The structures for the liberated CO and $Ph_3SiH$ (**C**) are not shown.

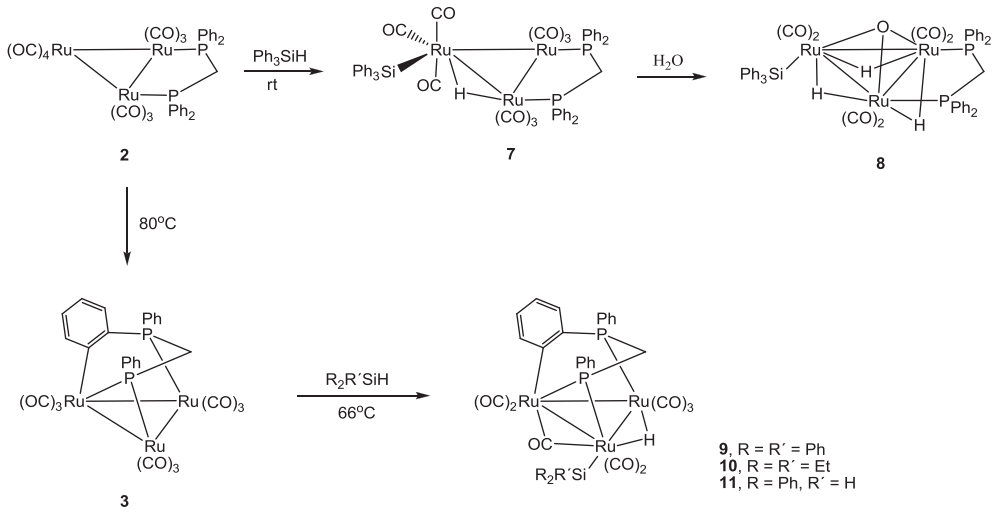


**Scheme 3.**

$Ru_2(CO)_6(\mu\text{-dppm})(\mu\text{-Sitol}_2)$ and $Ru_2(CO)_5(Sitol_2H)(\mu\text{-dppm})(\mu\text{-}\eta^2\text{-HSitol}_2)$ [14], treatment with excess $Ph_3SiH$ at room temperature is accompanied by loss of CO ligand and oxidative addition of silane to afford the silyl cluster $Ru_3(CO)_9(\mu\text{-dppm})(SiPh_3)(\mu\text{-H})$ (**7**) in 40% yield, in addition to the trihydrido oxo-capped silyl compound $Ru_3(\mu_3\text{-O})(\mu\text{-dppm})(CO)_6(SiPh_3)(\mu\text{-H})$ (**8**) (15% yield). Interestingly, in solution **7** slowly converts back to **2** by addition of CO to the putative cluster $Ru_3(CO)_9(\mu\text{-dppm})$, whose formation is expected upon reductive elimination of $Ph_3SiH$ from **7**. Here the extra CO needed for the regeneration of **2** is presumed to originate from cluster degradation. Compound **8** was neither observed in the solution at the start of the reaction nor in the crude product before chromatographic separation. In separate experiment we found that **7** reacts with $H_2O$ to yield **8**, suggesting that the latter being formed on the TLC plate from the reaction between **7** and $H_2O$ present in the chromatographic support. Examples of $\mu_3$-oxo triruthenium carbonyl clusters are relatively rare. The triruthenium clusters $Ru_3(CO)_8(\mu\text{-dppm})_2$, $Ru_3(CO)_6(\mu\text{-dppm})_3$ and $Ru_3(CO)_9(\mu\text{-dppm})\{P(C_4H_3S)_3\}$ react with molecular oxygen at elevated temperatures to yield oxo-capped $Ru_3(\mu_3\text{-O})(\mu_3\text{-CO})(CO)_5(\mu\text{-dppm})_2$ [43], $Ru_3(\mu_3\text{-O})(\mu_3\text{-CO})(CO)_3(\mu\text{-dppm})_3$ [44] and $Ru_3(\mu_3\text{-O})(\mu_3\text{-CO})(CO)_6(\mu\text{-dppm})\{P(C_4H_3S)_3\}$ [45], respectively. Although **2** exhibits rich and diverse chemistry with respect to substrate activation [21], its reaction with molecular oxygen is unknown and, to our knowledge, compound **8** represents the first example of an oxo-capped triruthenium carbonyl cluster containing a single dppm ligand as the phosphine auxiliary.

We were unable to grow X-ray quality crystals of **7**; therefore, its characterization was based on elemental analysis, infrared, $^1H$ NMR, $^{31}P\{^1H\}$ NMR and mass spectral data. The FAB mass spectrum displays a molecular ion peak at *m/z* 1201. The carbonyl stretching frequencies of **7** are similar to those of $Ru_3(CO)_9(\mu\text{-dppf})(SiPh_3)(\mu\text{-H})$ (**4**), indicating that the two clusters have a similar distribution of carbonyl ligands. The $^1H$ NMR spectrum shows, in addition to the resonances corresponding to the phenyl protons of the dppm and silyl ligands, a triplet at $\delta$ 4.47 that is assigned to the methylene protons of the dppm ligand, along with a high-field doublet at $\delta$ −18.10 for the bridging hydride. This latter resonance is coupled to one of the neighboring non-equivalent phosphorus nuclei, one of which is assumed to be *cis* (geminal) to the hydride ligand based on a $J_{P-H}$ of 32 Hz. A similar $J_{P-H}$ coupling constant has been reported for the structurally characterized osmium analog $Os_3(CO)_9(\mu\text{-dppm})(SiPh_3)(\mu\text{-H})$ ($J_{P-H}$ 30.4 Hz) [19]. The $^{31}P\{^1H\}$ NMR spectrum of **7** shows two doublets at $\delta$ 10.4 and 8.9 ($J_{P-P}$ 45.3 Hz) for the two non-equivalent $^{31}P$ atoms of dppm ligand, both of which are equatorially bonded to adjacent Ru atoms. These $^{31}P$ NMR data mirror those results found in the osmium analog $Os_3(CO)_9(\mu\text{-dppm})(SiPh_3)(\mu\text{-H})$ ($J_{P-P}$ 46.5 Hz), whose $SiPh_3$ ligand adopts an equatorial site proximal to the hydride. [19] Cluster **7** contains 48 valence electrons, and each ruthenium atom formally has an 18-electron configuration. Given the spectroscopic similarity of **7** to $Os_3(CO)_9(\mu\text{-dppm})(SiPh_3)(\mu\text{-H})$ [19], the hydride in **7** is assumed to bridge one of the unsupported Ru—Ru edges. This is consistent with our previous observations that the dppm-bridged Ru—Ru edge in **7** does not have enough room to accommodate both the hydride and the dppm ligand at a common edge [46].

The molecular structure of **8** is shown in Fig. 5, and selected bond angles and lengths are listed in the caption. The molecule

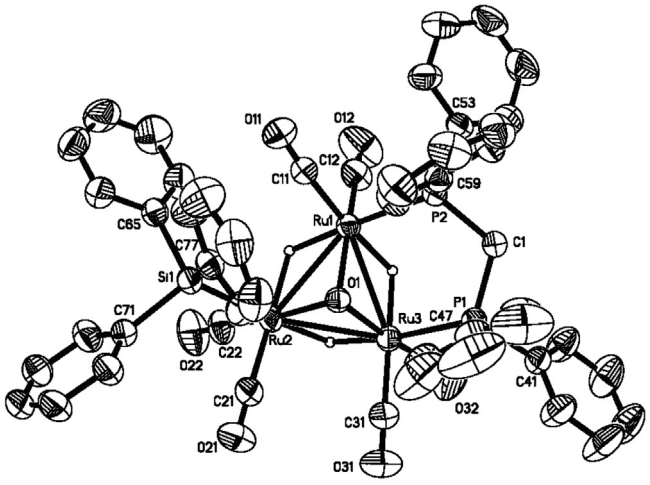


**Fig. 5.** ORTEP diagram of the molecular structure of $Ru_3(CO)_6(\mu_3\text{-O})(\mu\text{-dppm})(SiPh_3(\mu\text{-H})_3$ (**8**). Hydrogen atoms except those directly bonded to metals are omitted for clarity. Selected bond lengths (Å) and angles (°): Ru(1)–Ru(2) 2.8409(3), Ru(2)–Ru(3) 2.8335(3), Ru(1)–Ru(3) 2.8272(3), Ru(1)–P(2) 2.3477(6), Ru(3)–P(1) 2.3492(6), Ru(1)–O(1) 2.0506(15), Ru(2)–O(1) 2.0561(15), Ru(3)–O(1) 2.0701(16), Ru(2)–Si(1) 2.4142(7), Ru(1)–Ru(3)–Ru(2) 60.247(8), Ru(3)–Ru(1)–Ru(2) 59.98(7), Ru(3)–Ru(2)–Ru(1) 59.766(7), Ru(1)–O(1)–Ru(3) 86.64(6), Ru(1)–O(1)–Ru(2) 87.54(6), Ru(2)–O(1)–Ru(3) 86.74(6), O(1)–Ru(1)–Ru(3) 46.97(4), O(1)–Ru(1)–Ru(2) 46.31(4), O(1)–Ru(3)–Ru(1) 46.39(4), O(1)–Ru(3)–Ru(2) 46.42(4), O(1)–Ru(2)–Ru(3) 46.84(4), O(1)–Ru(2)–Ru(1) 46.15(4), O(1)–Ru(2)–Si(1) 98.99(5), Si(1)–Ru(2)–Ru(3) 145.8(2).

consists of a triangular framework of ruthenium atoms, where one of the polyhedral faces is best viewed as symmetrically capped by the triply bridging oxo-ligand [Ru(1)–O(1) 2.0506(15), Ru(2)–O(1) 2.0561(15), Ru(3)–O(1) 2.0701(16) Å]. The other ligands in **8** consist of a bridging dppm group, a terminally coordinated triphenylsilyl group, and six terminal carbonyl groups. The Ru(1)–Ru(3) bond [2.8272(3) Å] bridged by the dppm ligand is slightly shorter than the distance of other two Ru–Ru bonds [Ru(1)–Ru(2) 2.8409(3), Ru(2)–Ru(3) 2.8335(3) Å], and these Ru–Ru distances are in accordance with their single bond designation. The Ru–Si bond distance of 2.4142(7) Å is comparable to that found in **4**. The dppm ligand occupies equatorial sites in the cluster and the Ru–P distances [Ru(1)–P(2) 2.3477(6) and Ru(3)–P(1) 2.3492(6) Å], which are almost equal in length, are unexceptional relative to the Ru–P distances in **2** [2.322(2) and 2.334(2) Å] [47]. The three hydride ligands bridging three ruthenium–ruthenium edges were crystallographically located but not refined. Their positions, as shown in Scheme 3, are confidently assigned on the basis of the NMR data (*vide infra*). Significantly, the Ru–P vectors do not lie significantly out of the equatorial plane that is defined by the metal triangle. The disposition of the hydrides and the O(1) oxo atom are situated *trans* to each other, and these groups reside on opposite sides of the metallic plane. The triruthenium framework of **8** is comparable with those oxo-capped clusters $Ru_3(\mu_3\text{-}O)(C_6H_2Me_4)_3(\mu\text{-}H)_3^+$ [48], $Ru_3(\mu_3\text{-}O)(C_6H_6)(C_6Me_6)_2(\mu\text{-}H)_3^+$ [49], and $Ru_3(\mu_3\text{-}O)(Fc\text{-arene})(C_6Me_6)_2(\mu\text{-}H)_3^+$ [50], showing similar polyhedral architecture and arrangement of the oxo and hydride ligands.

The spectroscopic data for **8** are fully consistent with the solid-state structure. The IR spectrum exhibits four terminal $\nu$(CO) bands over the region of 2040–1946 $cm^{-1}$. The FAB mass spectrum displays a molecular ion peak at *m/z* 1135, along with fragmentation peaks corresponding to the loss of up to six carbonyl groups. The $^{31}P\{^1H\}$ NMR spectrum displays two doublets at $\delta$ 27.9 and 24.1 (*J* 61.0 Hz), indicating that **8** contains two non-equivalent phosphorus nuclei. In addition to the phenyl proton resonances of the dppm and $Ph_3Si$ ligands in the aromatic region, the $^1H$ NMR spectrum shows two multiplets at $\delta$ 3.51 and 3.04 that are assigned to the diastereotopic methylene protons of the diphosphine ligand, as well as three distinct hydride resonances (each integrating for 1H) that appear as two doublets at $\delta$ −11.75 (*J* 74.4 Hz) and $\delta$ −14.56 (*J* 60 Hz), and a broad singlet at $\delta$ −16.08.

The reactivity of **2** with $Et_3SiH$ and $Ph_2SiH_2$ was also investigated. Unfortunately, the addition of excess $Et_3SiH$ or $Ph_2SiH_2$ to a $CH_2Cl_2$ solution of **2** led to the rapid formation of unidentified decomposition products. Attempts to isolate the reaction products were not successful. The silyl-substituted cluster products that are formed here are less stable than **7**.

### 3.3. Oxidative addition of H–Si bonds to $Ru_3(CO)_9\{\mu_3\text{-}PPhCH_2PPh(C_6H_4)\}$ (**3**)

In order to compare the chemistry of the orthometalated derivative **3** with that of the parent cluster **2**, we investigated the reactions of **3** with silanes. The orthometalated compound **3** does not react with $Ph_3SiH$, $Et_3SiH$ and $Ph_2SiH_2$ at room temperature, but it does react at 66 °C to give $Ru_3(\mu\text{-}CO)(CO)_7\{\mu_3\text{-}PPhCH_2PPh(C_6H_4)\}(SiR_2R')(\mu\text{-}H)$ (**9**, R = R′ = Ph, 71% yield; **10**, R = R′ = Et, 60% yield; **11**, R = Ph, R′ = H, 66% yield) (Scheme 3). Compounds **9**–**11** have been characterized by a combination of spectroscopic methods, and the molecular structures determined by X-ray crystallography. The solid-state structures of the isostructural clusters **9**–**11** are depicted in Figs. 6–8, respectively, with the captions containing selected bond distances and angles. The basic cores of the three clusters are the same, having a triangular metal-framework of ruthenium atoms and three

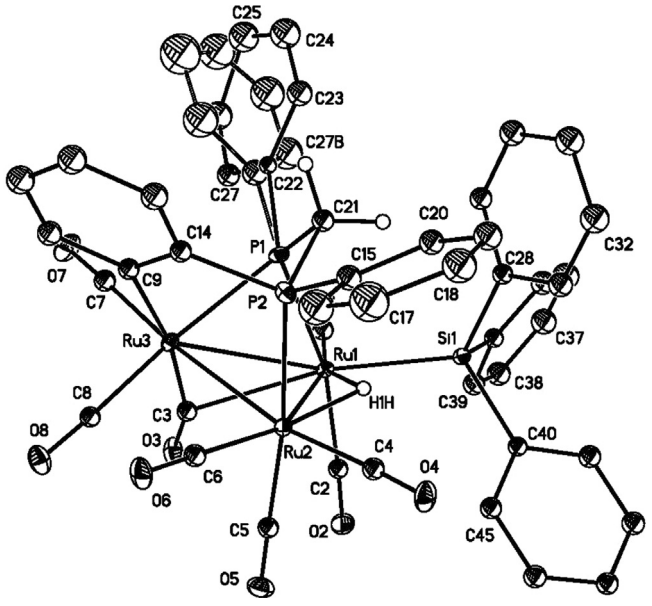


**Fig. 6.** ADP drawing of the molecular unit of $Ru_3(\mu\text{-}CO)(CO)_7(\mu_3\text{-}\eta^3\text{-}PhPCH_2PPh(C_6H_4)(SiPh_3)(\mu\text{-}H)$ (**9**). Ring hydrogen atoms are omitted for clarity. Selected bond lengths (Å) and angles (°): Ru(1)–Ru(2) 3.0537(5), Ru(2)–Ru(3) 2.8675(4), Ru(1)–Ru(3) 2.9702(4), Ru(1)–P(1) 2.332(1), Ru(2)–P(2) 2.353(1), Ru(3)–P(1) 2.404(11), Ru(1)–Si(1) 2.4254(12), Ru(1)–C(3) 2.564(4), Ru(3)–C(3) 1.968(4); Ru(1)–Ru(2)–Ru(3) 60.117(10), Ru(2)–Ru(3)–Ru(1) 63.053(11), Ru(3)–Ru(1)–Ru(2) 56.830(10), Ru(1)–P(1)–Ru(3) 77.67(3), P(1)–Ru(1)–Ru(2) 78.78(3), P(1)–Ru(1)–Ru(3) 52.25(3), P(1)–Ru(3)–Ru(1) 50.08(3), P(1)–Ru(3)–Ru(2) 81.62(3), P(2)–Ru(2)–Ru(3) 76.69(3), P(2)–Ru(2)–Ru(1) 93.74(3), P(1)–Ru(1)–Si(1) 106.24(4), Si(1)–Ru(1)–Ru(3) 153.14(3), Ru(3)–C(3)–Ru(1) 80.62(15), Ru(3)–C(3)–O(3) 158.8(4), Ru(1)–C(3)–O(3) 120.6(3).

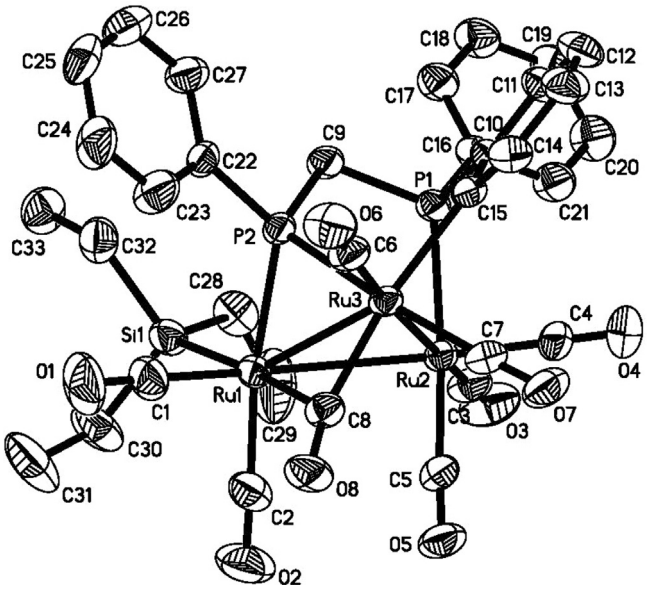


**Fig. 7.** ORTEP diagram of the molecular structure of $Ru_3(\mu\text{-}CO)(CO)_7(\mu_3\text{-}\eta^3\text{-}PhPCH_2PPh(C_6H_4)(SiEt_3)(\mu\text{-}H)$ (**10**). Hydrogen atoms are omitted for clarity. Selected bond lengths (Å) and angles (°): Ru(1)–Ru(2) 3.0159(9), Ru(2)–Ru(3) 2.8521(7), Ru(1)–Ru(3) 2.9706(7), Ru(1)–P(2) 2.3276(12), Ru(3)–P(2) 2.3939(11), Ru(2)–P(1) 2.3563(11), Ru(1)–Si(1) 2.405(2), Ru(1)–C(8) 2.505(4), Ru(3)–C(8) 1.971(4); Ru(1)–Ru(2)–Ru(3) 60.750(13), Ru(2)–Ru(1)–Ru(3) 56.899(15), Ru(2)–Ru(3)–Ru(1) 62.35(2), Ru(1)–P(2)–Ru(3) 77.96(3), P(2)–Ru(1)–Ru(3) 52.01(3), P(2)–Ru(3)–Ru(1) 50.02(3), P(1)–Ru(2)–Ru(3) 77.35(3), P(1)–Ru(2)–Ru(1) 93.25(3), P(2)–Ru(1)–Si(1) 93.92(9), Ru(1)–C(8)–Ru(3) 82.22(13), Ru(1)–C(8)–O(8) 121.0(3), Ru(3)–C(8)–O(8) 156.7(4).

distinctly different ruthenium–ruthenium bond lengths [Ru(1)–Ru(2) 3.0537(5), Ru(2)–Ru(3) 2.8675(4), Ru(1)–Ru(3) 2.9702(4) Å for **9**; Ru(1)–Ru(2) 3.0159(9), Ru(2)–Ru(3) 2.8521(7), Ru(1)–Ru(3) 2.9706(7) Å for **10**; Ru(1)–Ru(2) 2.9822(6), Ru(2)–Ru(3) 2.8344(6), Ru(1)–Ru(3) 2.9544(6) Å for **11**]. Of the seven terminal carbonyl ligands, two each are located at the Ru(1) and Ru(3) centers, and three at the Ru(2) atom. The three products each exhibit one semi-bridging carbonyl ligand involving the Ru(1) and Ru(3) atoms [Ru(1)–C(3) 2.564(4), Ru(3)–C(3) 1.968(4) Å, Ru(3)–C(3)–O(3) 158.8(4)° for **9**; Ru(1)–C(8) 2.505(4), Ru(3)–C(8) 1.971(4) Å, Ru(3)–C(8)–O(8) 156.7(4)° for **10** and Ru(1)–C(8) 2.565(3), Ru(3)–C(8) 1.950(4) Å, Ru(3)–C(8)–O(8) 159.9(9)° for **11**]. The silyl groups are terminally bound to the Ru(1) atom and the Ru–Si bond distances [Ru(1)–Si(1) 2.4254(12) Å for **9**; Ru (1)–Si(1) 2.405(2) Å for **10** and Ru(1)–Si(1) 2.3829(10) Å for **11**] are very similar to those found in **4** and **8**. The hydride ligand in **9**, which was located using the program WinGX, is associated with the longest ruthenium–ruthenium edge [Ru(1)–Ru(2) 3.0537(5) Å]. Significantly, the $SiPh_3$ ligand is *cis* to the hydride at the sterically least crowded equatorial site. The hydrides for **10** and **11** could not be crystallographically located but their position, as shown in Scheme 3, is confidently inferred from the NMR data. The tridentate phosphine ligand in **9** maintains the same coordination mode as that found in the parent cluster **3** [22a]. The product contains three Ru–Ru single bonds and possesses a closed-shell configuration with an 18-electron count at each Ru atom.

The solution spectroscopic data for **9**–**11** are consistent with the solid-state structure of each product. The IR spectrum of each compound exhibits, in addition to five terminal $\nu$CO bands, an absorption at lower wave number (1863 w $cm^{-1}$ for **9**; 1869 w $cm^{-1}$ for **10**; 1867 w $cm^{-1}$ for **11**), that supports the presence of a semi-bridging carbonyl group. The $^{31}P\{^1H\}$ NMR spectrum for each compound displays two doublets [$\delta$ 88.6, −0.73 ($J$ 81.9 Hz) for **9**, $\delta$ 80.9, −0.09 ($J$ 82.5 Hz) for **10**, and $\delta$ 89.7, −1.5 ($J$ 78.3 Hz) for **11**], consistent with the solid-state structures. In addition to the aryl resonances from the diphosphine and silyl ligands, each $^1H$ NMR spectrum shows two multiplets in the aliphatic region ($\delta$ 3.75 and 4.43 for **9**; $\delta$ 3.13 and 3.77 for **10**; $\delta$ 2.56 and 2.85 for **11**) that are assigned to the diastereotopic methylene protons of the diphosphine ligand. Finally, each cluster exhibits a single high-field hydride ($\delta$ −16.10 for **9** and −16.50 for **10**; −16.39 for **11**) as a result of silane activation.

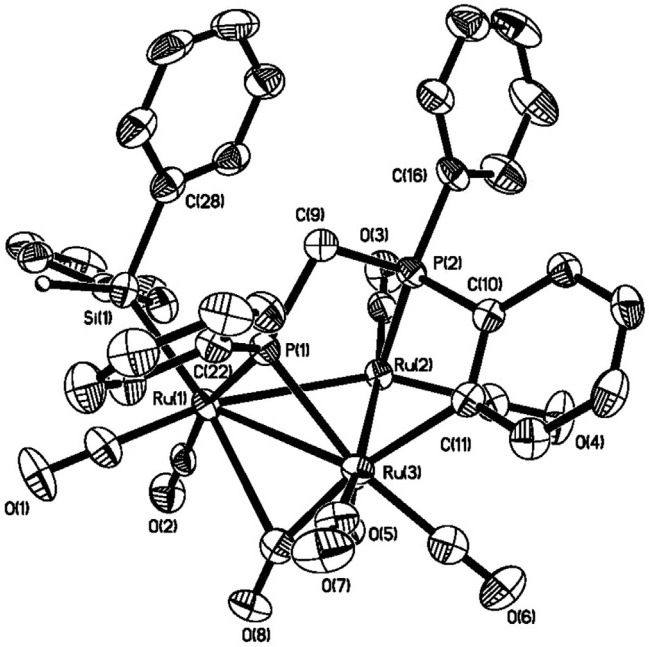


**Fig. 8.** ORTEP drawing of the molecular unit of $Ru_3(\mu\text{-CO})(CO)_7\{\mu_3\text{-}\eta^3\text{-}PPhCH_2PPh(C_6H_4)\}(Ph_2SiH)(\mu\text{-H})$ (**11**). Hydrogen atoms (except that bonded to silane) are omitted for clarity. Selected bond lengths (Å) and angles (°): Ru(1)–Ru(2) 2.9822(6), Ru(2)–Ru(3) 2.8344(6), Ru(1)–Ru(3) 2.9544(6), Ru(1)–Si(1) 2.3829(10), Ru(1)–P(1) 2.3107(9), Ru(2)–P(2) 2.3448(9), Ru(3)–P(1) 2.3724(10), Ru(1)–C(8) 2.565(3), Ru(3)–C(8) 1.950(4); Ru(2)–Ru(3)–Ru(1) 61.978(10), Ru(3)–Ru(2)–Ru(1) 60.987(16), Ru(3)–Ru(1)–Ru(2) 57.035(13), P(1)–Ru(1)–Si(1) 99.02(3), Si(1)–Ru(1)–C(8) 171.25(8), P(1)–Ru(1)–Ru(3) 51.82(3), Si(1)–Ru(1)–Ru(3) 147.51(3), P(1)–Ru(1)–Ru(2) 79.27(3), Si(1)–Ru(1)–Ru(2) 109.03(3), C(8)–Ru(1)–Ru(2) 78.30(7), P(2)–Ru(2)–Ru(3) 77.62(2), P(2)–Ru(2)–Ru(1) 94.00(3), C(8)–Ru(3)–P(1) 101.49(10), P(1)–Ru(3)–Ru(2) 81.47(2), P(1)–Ru(3)–Ru(1) 49.97(2), Ru(1)–P(1)–Ru(3) 78.21.

## 4. Conclusions

The reactions described in this study are summarized in Schemes 2 and 3. As described in the introduction, oxidative addition of Si–H bonds to $Ru_3(CO)_{12}$ was investigated in early 1970s; however, the reactions with trialkyl silanes typically induced the cleavage and recombination of ruthenium–ruthenium bonds in the initially formed products to yield silyl-substituted ruthenium complexes with lower nuclearity [6]. Successful formation of the trinuclear oxidative-addition products **4**–**6** from the reactions of **1** with $Ph_3SiH$, $Et_3SiH$ and $Ph_2SiH_2$ can be attributed to the fact that the dppf ligand in **4**–**6** helps to suppress cluster fragmentation. The reaction of **2** with $Ph_3SiH$ gives **7**, which is isostructural with $Os_3(CO)_9(\mu\text{-dppm})(SiPh_3)(\mu\text{-H})$ reported by us earlier [19], reacts with $H_2O$ to give the oxo-capped cluster **8**. The reaction of **2** with hydrosilanes yields products of differing stability, and only in the case of $Ph_3SiH$ was the oxidative-addition product **8** found to be stable. The dppf analog of **8** was not formed from **4** during chromatography indicating greater stability of the dppf bridged molecules compared to those bridged by dppm. This stands in contrast to the reaction of the orthometalated compound **3** and silanes, which affords the isostructural hydride clusters **9**–**11** through activation of the silane reagent. Clusters **1** and **2** maintain their nuclearity, even after significant substrate activation involving the oxidative cleave of Si–H bonds in hydrosilanes, a process of fundamental importance in hydrosilation catalysis, because of the stabilizing effect the small bite angle ligands dppf and dppm exert on the cluster frame. Future studies will probe the catalytic activity of these clusters in the hydrosilylation of organic substrates.

## Acknowledgments

This research has been partly sponsored by the Ministry of Education, Government of the People's Republic of Bangladesh. SG thanks Commonwealth Commission for a scholarship. We gratefully acknowledge Prof. A.J. Deeming and our deceased friend Prof. D.T. Haworth for collecting XRD data of cluster **8** and **10** respectively. Financial support from the Robert A. Welch Foundation (Grant B-1093-MGR) and the NSF (CHE-0741936) are acknowledged. We also thank Prof. Michael B. Hall (TAMU) for providing us a copy of his *JIMP2* program.

## Appendix A. Supplementary material

CCDC 997408, 923714, 921503, 956408 and 997409 contain the supplementary crystallographic data for this paper. These data can be obtained free of charge from The Cambridge Crystallographic Data Centre via www.ccdc.cam.ac.uk/data_request/cif. Atomic

coordinates of all optimized structures are available from MGR upon request.

## References


[1] U. Schubert, Adv. Organomet. Chem. 30 (1990) 151–187.
[2] (a) F.L. Taw, R.G. Bergmam, M. Brookhart, 23 (2004) 886–890. (b) J.L. Speier, Adv. Organomet. Chem. 17 (1979) 407–447;
(c) B. Marciniec, J. Gulinski, W. Urbaniak, Z.W. Kornetka, in: B. Marciniec (Ed.), Comprehensive Handbook on Hydrosilylation, Pergamon Press, Oxford, 1992, pp. 49–62 and 88–93;
(d) B. Marciniec, J. Gulinski, J. Organomet. Chem. 446 (1993) 15–23.
[3] A.A. Bengali, R. Fehnel, Organometallics 24 (2005) 1156–1160.
[4] (a) Z. Lin, Chem. Soc. Rev. 31 (2002) 239–245;
(b) J.Y. Corey, J. Braddock-Wilking, Chem. Rev. 99 (1999) 175–292;
(c) I. Ojima, in: S. Patai, Z. Rappoport (Eds.), The Chemistry of Organic Silicon Compounds, vol. 2, Wiley Interscience, New York, 1989, pp. 1479–1526. Chapter 25;
(d) J. Schneider, J. Angew. Chem. Int. Ed. Engl. 35 (1996) 1068–1075;
(e) P. Braunstein, M. Knorr, J. Organomet. Chem. 500 (1995) 21–38;
(f) J.Y. Corey, Chem. Rev. 111 (2011) 863–1071.
[5] (a) G.N. Buuren, A.C. Willis, W.B. Einstein, R.K. Peterson, R.K. Pomeroy, D. Sutton, Inorg. Chem. 20 (1981) 4361–4367;
(b) A. Brookes, S.A.R. Knox, F.G.A. Stone, J. Chem. Soc. A (1971) 3469–3471;
(c) S.A.R. Knox, F.G.A. Stone, J. Chem. Soc. A (1969) 2559–2565;
(d) L. Vancea, W.A.G. Graham, Inorg. Chem. 13 (1974) 511–513;
(e) S. Kotani, T. Tanizawa, T. Adachi, T. Yoshida, K. Sonogashira, Chem. Lett. 23 (1994) 1665–1668.
[6] P. Braunstein, J.R. Galsworthy, W. Massa, J. Chem. Soc. Dalton Trans. (1997) 4677–4681.
[7] K. Burgess, C. Guerin, B.F.G. Johnson, J. Lewis, J. Organomet. Chem. 295 (1985) C3–C6.
[8] (a) G. Süss-Fink, J. Ott, B. Schmidkonz, K. Guldner, Chem. Ber. 115 (1982) 2487–2491;
(b) H.P. Klein, U. Thewalt, G. Herrmann, G. Süss-Fink, C. Moinet, J. Organomet. Chem. 286 (1985) 225–236.
[9] J.A. Cabeza, A. Llamazares, V. Riera, S. Triki, L. Ouahab, Organometallics 11 (1992) 3334–3339.
[10] J.A. Cabeza, R.J. Franco, A. Llamazares, V. Riera, C. Bois, Y. Jeannin, Inorg. Chem. 32 (1993) 4640–4642.
[11] J.A. Cabeza, S. Garcia-Granda, A. Llamazares, V. Riera, J.F. Van der Maelen, Organometallics 12 (1993) 2973–2979.
[12] H. Nagashima, A. Suzuki, T. Iura, K. Ryu, K. Matsubara, Organometallics 19 (2000) 3579–3590.
[13] K. Matsubara, K. Ryu, T. Maki, T. Iura, H. Nagashima, Organometallics 21 (2002) 3023–3032.
[14] R.D. Adams, B. Captain, W. Fu, Organometallics 19 (2000) 3670–3673.
[15] (a) R.D. Adams, J.E. Cortopassi, M.P. Pompeo, Inorg. Chem. 30 (1991) 2960–2961;
(b) R.D. Adams, J.E. Cortopassi, M.P. Pompeo, Inorg. Chem. 31 (1992) 2563–2568.
[16] B.F.G. Johnson, J. Lewis, M. Monari, D. Braga, F. Grepioni, C. Gradella, J. Chem. Soc. Dalton Trans. (1990) 2863–2871.
[17] R.J. Hall, P. Serguievski, J.B. Keister, Organometallics 19 (2000) 4499–4505.
[18] F.W.B. Einstein, R.K. Pomeroy, A.C. Wills, J. Organomet. Chem. 311 (1986) 257–268.
[19] A.J. Deeming, M.M. Hassan, S.E. Kabir, E. Nordlander, D.A. Tocher, Dalton Trans. (2004) 3709–3714.
[20] H. Hashimoto, Y. Hayashi, I. Aratani, C. Kabuto, M. Kira, Organometallics 21 (2002) 1534–1536.
[21] S.E. Kabir, G. Hogarth, Coord. Chem. Rev. 253 (2009) 1285–1315 and references cited therein.
[22] (a) N. Lugan, J.-J. Bonnet, J.A. Ibers, J. Am. Chem. Soc. 107 (1985) 4484–4491;
(b) M.I. Bruce, P.A. Humphrey, B.W. Skelton, A.H. White, M.L. Williams, Aust. J. Chem. 38 (1985) 1301–1306;
(c) M.I. Bruce, J.G. Martisos, B.K. Nicholson, J. Organomet. Chem. 247 (1983) 321–338;
(d) M.I. Bruce, O. Bin Shawkataly, M.L. Williams, J. Organomet. Chem. 287 (1985) 127–131;
(e) S.E. Kabir, M.R. Hassan, D.T. Haworth, S.V. Lindeman, T.A. Siddiquee, D.W. Bennett, J. Organomet. Chem. 692 (2007) 3936–3943;
(f) M.I. Bruce, J.R. Hinchliffe, R. Surynt, B.W. Skelton, A.H. White, J. Organomet. Chem. 469 (1994) 89–97;
(g) C.J. Cardin, D.J. Cardin, M.A. Convery, Z. Dauter, D. Fenske, M.M. devereux, M.B. Power, J. Chem. Soc. Dalton Trans. (1996) 1133–1144;
(h) N. Begum, MdI. Hyder, M.R. Hassan, S.E. Kabir, D.W. Bennett, D.T. Haworth, T.A. Siddiquee, D. Rokhsana, A. Sharmin, E. Rosenberg, Organometallics 27 (2008) 1550–1560;
(i) C.J. Adams, M.I. Bruce, O. Kühl, B.W. Skelton, A.H. White, J. Organomet. Chem. 445 (1993) C6–C9;
(j) C.J. Adams, M.I. Bruce, P.A. Duckworth, P.A. Humphrey, O. Kühl, B.W. Skelton, A.H. White, J. Organomet. Chem. 467 (1994) 251–281.
[23] M.N. Uddin, N. Begum, M.R. Hasan, G. Hogarth, S.E. Kabir, M.A. Miah, E. Nordlander, D.A. Tocher, Dalton Trans. (2008) 6219–6230.
[24] M.I. Bruce, P.A. Humphrey, O. Bin Shawkataly, M.R. Snow, E.R.T. Tiekink, W.R. Cullen, Organometallics 9 (1990) 2910–2919.
[25] MdK. Hossain, S. Rajbangshi, A. Rahaman, M.A.H. Chowdhury, T.A. Siddiquee, S. Ghosh, M.G. Richmond, E. Norlander, G. Hogarth, S.E. Kabir, J. Organomet. Chem. 760 (2014) 231–239.
[26] N. Begum, U.K. Das, M. Hassan, G. Hogarth, S.E. Kabir, E. Nordlander, Md A. Rahman, D.A. Tocher, Organometallics 26 (2007) 6462–6472.
[27] M.I. Bruce, B.K. Nicholson, M.L. Williams, Inorg. Synth. 26 (1990) 265–280.
[28] SMART and SAINT+ Software for CCDC Diffractometers, Version 6.1, Bruker AXS Inc., Madison, WI, 2000.
[29] G.M. Sheldrick, SHELXTL PLUS, Version 6.1, Bruker AXS, Madison, WI, 2000.
[30] SMART Version 5.628, Bruker AXS, Inc., Madison, WI, 2003.
[31] SAINT Version 6.36, Bruker AXS, Inc., Madison, WI, 2002.
[32] G. Sheldrick, SADABS Version 2.10, University of Göttingen, 2003.
[33] SHELXTL V6.12, Bruker AXS, Inc., Madison, WI, 2003.
[34] J.L. Farrugia, J. Appl. Crystallogr. 32 (1999) 837–838.
[35] A.J.C. Wilson (Ed.), International Tables for X-ray Crystallography, vol. C, Kynoch, Academic Publishers, Dordrecht, 1992. Tables 6.1.1.4 (pp. 500–502) and 4.2.6.8 (pp. 219–222).
[36] M. Svensson, S. Humbel, R.D.J. Froese, T. Matsubara, S. Sieber, K. Morokuma, J. Phys. Chem. 100 (1996) 19357–19363.
[37] M.J. Frisch, G.W. Trucks, H.B. Schlegel, G.E. Scuseria, M.A. Robb, J.R. Cheeseman, G. Scalmani, V. Barone, B. Mennucci, G.A. Petersson, H. Nakatsuji, M. Caricato, X. Li, H.P. Hratchian, A.F. Izmaylov, J. Bloino, G. Zheng, J.L. Sonnenberg, M. Hada, M. Ehara, K. Toyota, R. Fukuda, J. Hasegawa, M. Ishida, T. Nakajima, Y. Honda, O. Kitao, H. Nakai, T. Vreven, J.A. Montgomery Jr., J.E. Peralta, F. Ogliaro, M. Bearpark, J.J. Heyd, E. Brothers, K.N. Kudin, V.N. Staroverov, R. Kobayashi, J. Normand, K. Raghavachari, A. Rendell, J.C. Burant, S.S. Iyengar, J. Tomasi, M. Cossi, N. Rega, J.M. Millam, M. Klene, J.E. Knox, J.B. Cross, V. Bakken, C. Adamo, J. Jaramillo, R. Gomperts, R.E. Stratmann, O. Yazyev, A.J. Austin, R. Cammi, C. Pomelli, J.W. Ochterski, R.L. Martin, K. Morokuma, V.G. Zakrzewski, G.A. Voth, P. Salvador, J.J. Dannenberg, S. Dapprich, A.D. Daniels, O. Farkas, J.B. Foresman, J.V. Ortiz, J. Cioslowski, D.J. Fox, Gaussian 09, Revision A.02, Gaussian, Inc., Wallingford CT, 2009.
[38] (a) JIMP2, version 0.091, a free program for the visualization and manipulation of molecules: M.B. Hall, R.F. Fenske, Inorg. Chem. 11 (1972) 768–775;
(b) J. Manson, C.E. Webster, M.B. Hall, Texas A&M University, College Station, TX, 2006. http://www.chem.tamu.edu/jimp2/index.html.
[39] S.T. Chacon, W.R. Cullen, M.I. Bruce, O.B. Shawkataly, F.W.B. Einstein, R.H. Jones, A.C. Willis, Can. J. Chem. 68 (1990) 2001–2010.
[40] Md A. Rahman, N. Begum, S. Ghosh, Md K. Hossain, G. Hogarth, D.A. Tocher, E. Nordlander, S.E. Kabir, J. Organomet. Chem. 696 (2011) 607–611.
[41] A.A. Torabi, A.S. Humphreys, G.A. Koutsantonis, B.W. Skelton, A.W. White, J. Organomet. Chem. 655 (2002) 227–232.
[42] J.W. Akitt, B.E. Mann, NMR and Chemistry, Stanley Thornes, UK, 2000.
[43] A. Colombie, J.-J. Bonnet, P. Fompeyrine, G. Lavigne, S. Sunshine, Organometallics 5 (1986) 1154–1159.
[44] H.A. Mirza, R.J. Puddephatt, J.J. Vittal, Z. Krist. New Cryst. Struct. 212 (1997) 411. Inorg. Chem. 34 (1995) 4239–4243.
[45] Md. D.H. Sikder, S. Ghosh, S.E. Kabir, G. Hogarth, D.A. Tocher, Inorg. Chim. Acta 376 (2011) 170–174.
[46] (a) S.E. Kabir, M.A. Miah, K. Uddin, A.J. Deeming, J. Organomet. Chem. 476 (1994) 121–126;
(b) A.J. Deeming, S.E. Kabir, J. Organomet. Chem. 340 (1988) 359–366.
[47] A.W. Coleman, D.F. Jones, P.H. Dixneuf, C. Brisson, J.J. Bonnet, G. Lavigne, Inorg. Chem. 23 (1984) 952–956.
[48] M.A. Bennett, T.-N. Huang, T.W. Matheson, A.K. Smith, Inorg. Synth. 21 (1982) 74–78.
[49] B. Therrien, L. Vieille-Petit, G. Süss-Fink, Inorg. Chim. Acta 357 (2004) 3289–3294.
[50] L. Vieille-Petit, S. Unternährer, B. Therrien, G. Süss-Fink, Inorg. Chim. Acta 355 (2003) 335–339.